



CHORUS

This is the accepted manuscript made available via CHORUS. The article has been published as:

Band gap and mobility of epitaxial perovskite $\text{BaSn}_{1-x}\text{Hf}_x\text{O}_3$ thin films

Juyeon Shin, Jinyoung Lim, Taewoo Ha, Young Mo Kim, Chulkwon Park, Jaejun Yu, Jae Hoon Kim, and Kookrin Char

Phys. Rev. Materials **2**, 021601 — Published 9 February 2018

DOI: [10.1103/PhysRevMaterials.2.021601](https://doi.org/10.1103/PhysRevMaterials.2.021601)

Bandgap and mobility of epitaxial perovskite $\text{BaSn}_{1-x}\text{Hf}_x\text{O}_3$ thin films

Juyeon Shin¹, Jinyoung Lim², Taewoo Ha³, Young Mo Kim¹, Chulkwon Park^{1*}, Jaejun Yu²,
Jae Hoon Kim³ and Kookrin Char^{1†}

¹*Institute of Applied Physics, Dept. of Physics and Astronomy, Seoul National University,
Seoul 08826, Korea, Republic of.*

²*Center for Theoretical Physics, Dept. of Physics and Astronomy, Seoul National University,
Seoul 08826, Korea, Republic of.*

³*Dept. of Physics, Yonsei University, Seoul 03722, Korea, Republic of.*

A wide bandgap perovskite oxide BaSnO_3 is attracting much attention due to its high electron mobility and oxygen stability. On the other hand, BaHfO_3 was recently reported to be an effective high-k gate oxide. Here we investigate the bandgap and mobility of solid solutions of $\text{BaSn}_{1-x}\text{Hf}_x\text{O}_3$ ($x=0-1$) (BSHO) as a basis to build advanced perovskite oxide heterostructures. All the films were epitaxially grown on MgO substrates using pulsed laser deposition. Density functional theory calculations confirmed that Hf substitution does not create mid-gap states while increasing the bandgap. From X-ray diffraction and optical transmittance measurements, the lattice constants and the bandgap values are significantly modified by Hf substitution. We also measured transport properties of n-type La-doped BSHO films ($(\text{Ba},\text{La})(\text{Sn},\text{Hf})\text{O}_3$), investigating the modulation doping feasibility in the BSO/BSHO heterostructures. The Hall measurement data revealed that, as the Hf content increases, the activation rate of La dopant decreases and the scattering rate of electrons sharply increases. These properties of BSHO films may be useful for application in various heterostructures based on the BaSnO_3 system.

* Currently at Samsung Electronics, Suwon, Korea

† To whom correspondence should be sent: kchar@phya.snu.ac.kr

A transparent perovskite oxide, BaSnO₃ (BSO), is attracting large interest due to its unusually high electron mobility (μ) at room temperature [1,2]. Single crystals of La-doped BSO were reported to exhibit high μ of 320 cm²V⁻¹s⁻¹ at the carrier density (n) of 8×10¹⁹ cm⁻³, the highest value among the wide band gap semiconductors in the degenerate doped regime [1,2]. The high μ of La-doped BSO single crystal is associated with the dispersive conduction band composed of Sn 5s orbital, the ideal 180° Sn-O-Sn bond angle, a large dielectric constant, and separation of SnO₂ layers from the La-doped BaO layers, etc [1]. However, epitaxial films exhibit reduced μ ranging from 10~183 cm²V⁻¹s⁻¹ [3-7], limiting the charge transport in heterostructure devices based on BSO. Since the lower μ is mainly attributed to the charge traps introduced by the high density of dislocations [8], many groups have extensively studied the electron transport in BSO films by suitable selections of the substrates and the deposition methods [3-7,9]. The highest mobility value in films reported to date is 183 cm²V⁻¹s⁻¹ at 1.2×10²⁰ cm⁻³ on a DyScO₃ substrate by molecular beam epitaxy [6].

Although the first requirement to achieve higher μ in BSO films is to reduce the scattering centers, the appropriate shielding of the charged scattering centers through local injection of high carrier density can enhance the electron transport beyond the current limit. Carrier modulation of the BSO channel by field effect has been studied with various solid state gate oxides, such as Al₂O₃, HfO₂, and epitaxial BaHfO₃ and LaInO₃, confirming the effective band bending in the metal-insulator-semiconductor structures with μ values ranging from 17.8 cm²V⁻¹s⁻¹ to ~ 90 cm²V⁻¹s⁻¹ [10-13]. Recently, μ was further improved to 300 cm²V⁻¹s⁻¹ at 50 K in an electric-double-layer transistor [14] by injecting electron carriers in undoped BSO. Other approaches to increase the carrier density in usual semiconductor devices are polarization [15] or modulation doped field effect transistors [16-18] and field effect transistors with high-k dielectrics [19]. The induced electric field and carriers even led to superconductivity [20]. To date in BSO, modulation doping, in which the transport electrons suffer less from ionized donor scattering due to spatial separation from the dopants, have not yet been studied.

To realize the modulation doped devices as in GaAs/AlGaAs, we need a larger bandgap material that can be grown epitaxially with BSO and does not perturb the crystal and band structure of BSO capable of generating the high μ . Since the bandgap of perovskite oxides are mostly driven by B-site cation and oxygen, substitution of Sn atoms in BSO may effectively change the band structure. On the other hand, substitution of A-site cations with other atoms usually distorts the cubic crystal structure of the perovskite oxide [21], so that the strain at the interface between the cubic BSO and non-cubic epitaxial layer might disturb the straight Sn-O-Sn bond. The previous research on the La-doped SrSnO₃ films found that only a few films are conductive [22,23] and reported the highest μ of 40 cm²V⁻¹s⁻¹ at 9×10^{19} cm⁻³ [24] with an increase of bandgap from 3.50 eV to 4.27 eV [25], implying the large effect of tilted and/or rotated SnO₆ octahedra on the electron transport. In the case of the B-site, Hf substitution on Sn-site can be a good candidate for the bandgap engineering of BSO. The cubic BaHfO₃ (BHO) has a slightly larger lattice constant (4.171 Å) than BSO (4.116 Å) and a larger optical gap of 6.1 eV [12]. The 2.6 eV increase of the bandgap with 4 % volume increase by B-site Hf substitution looks favorable compared to 0.77 eV increase of the bandgap with 8 % volume decrease by A-site Sr substitution. Meanwhile, recently the field effect mobility based on the BSO channel layer and the BHO gate oxide reached up to μ of 52.7 cm²V⁻¹s⁻¹, demonstrating their excellent interface property [12].

In this paper, we studied the bandgap and mobility behavior of BaSn_{1-x}Hf_xO₃ (x=0~1) (BSHO). The modified band structures by Hf substitution were investigated from density functional theory (DFT) calculations. The structure and optical properties of BSHO films from X-ray diffraction (XRD) and optical transmittance revealed that Hf substitution significantly change the lattice constant and the bandgap of BSO. We also investigated the transport properties of n-type La-doped BSHO films (BLSHO) to explore the modulation doping possibility in the BSO/BSHO heterostructure. The Hall measurement showed that BLSHO films are degenerate up to about 30 % substitution by Hf, appealing as a doping layer in a modulation doped heterostructure, although μ decreases upon Hf substitution.

All the films were grown on [001] MgO substrate using laser ablation method in an O₂ pressure of 0.1 Torr at 750 °C with 1.4~1.5 Jcm⁻² energy fluence. We deposited the BSHO films of 100 nm by sequential laser ablation of BSO and BHO targets for XRD and optical measurements. For all the compositions of La-doped BSHO films, we used sequential deposition of 2 or 3 targets from Ba_{0.99}L_{0.01}SnO₃, Ba_{0.96}L_{0.04}SnO₃, Ba_{0.96}L_{0.07}SnO₃, and BHO, while maintaining less than 1 unit cell thickness per each cycle.

First we calculated the band structure of BaSn_{1-x}Hf_xO₃ (x=0, 0.25, 0.5, 0.75, 1) in the scheme of the generalized gradient approximation with the revised Perdew-Burke-Ernzerhof functional for solids (GGA-PBESol) in DFT as implemented in the Vienna *ab initio* simulation package code [26]. This most commonly used version in solid-state calculations today was found to work well for perovskite oxides [27-28]. Fig. 1 shows the band structure and the total density of states (TDOS) /partial density of states (PDOS) per atom as varying Hf content. The 2×2×2 supercell is used for BaSn_{1-x}Hf_xO₃ (x=0.25, 0.5, 0.75) and the TDOS is scaled down to 1/8 to show each orbital characteristics effectively. The effective mass of conduction band is 0.2 m_0 for BSO and 0.62 m_0 for BHO, respectively, consistent with the previous calculations based on DFT [12,29]. Importantly, the substitution of Hf for Sn increases the band gap and do not create gap states, which is a crucial condition for bandgap engineering of BSO. Meanwhile, all the indirect bandgap calculations by unfolded Brillouin zone approach suggest that, while the O-2p orbital contribution continues to dominate near the valence band maximum (VBM), the feature of the conduction band minimum (CBM) abruptly changes. As the Hf content increases, the major contribution of the Sn-5s orbital decreases and the Hf-5d orbital becomes dominant in the CBM, decreasing the conduction band dispersion. The inset shows the enlarged PDOS plot only for Hf orbitals to show the characteristics in the conduction band edge (CBE). As the Hf content increases, the major contribution to CBE changes from the Hf-6s to the Hf-5d orbital, while the s orbital remains as the major contribution to CBE in the case of Sn.

We studied the structure properties of BSHO films by X-ray diffraction measurement, as shown in Fig. 2. The $\theta-2\theta$ scans in Fig. 2 (a) confirms the epitaxial growth of all the films on MgO substrate and the (002) BSHO peaks move toward the (002) peak of MgO substrate with increasing Hf content due to the larger lattice constant of BHO. The full widths at half-maximum (FWHM) of the ω -scan, presented in the inset, for $\text{BaSn}_{1-x}\text{Hf}_x\text{O}_3$ ($x=0.2, 0.4, 0.6$) films were smaller than for BSO on MgO, which is probably a consequence of better lattice matching with increasing Hf content. Due to proximity of the (002) peak of BHO to the substrate peak, we could not measure the ω -rocking curve around the (002) peak of $\text{BaSn}_{1-x}\text{Hf}_x\text{O}_3$ ($x=0.8, 1$) films. We also examined the in-plane lattice structure of BSO and BHO by the reciprocal space mapping (RSM) in Fig. 2 (b). Although the confined intensity in RSM indicates no polycrystalline growth, the larger spreads in the in-plane direction in both films suggest the high density of misfit dislocations as shown in Fig. S1 [7]. The large lattice mismatch of BSO (4.116 Å) compared to the MgO substrate (4.2 Å) generates the larger mosaicity in the in-plane direction than BHO (4.171 Å), involving the largest FWHM of 1.2° for the (002) peak of BSO in Fig. 2 (a). On MgO substrates, the structural quality improves as the Hf contents increases. Fig. 2 (c) describes the out-of-plane lattice constant of BSHO calculated from the $\theta-2\theta$ scans in Fig. 2 (a) and GGA-PBEsol with varying Hf contents. Conventionally, the lattice constant of alloy ($A_{1-x}B_x$) follows a linear equation conformable by the Vegard's law [30], that is,

$$a(x) = (1-x)a_A + xa_B \quad (1)$$

since the lattice parameter is determined by an ensemble average over a significant volume of the material. The lattice constants increase with more Hf content but the small deviation from the perfect linear line in the experimental result arises from the different degree of tensile strain (BSO: 4.126 Å, BHO: 4.168 Å in the in-plane direction) on MgO substrate, as exhibited in Fig. 2 (b).

We performed the optical transmittance measurement of BSHO films, as shown in Fig. 3 (a), in the range of 3~6.5 eV, which is smaller than the optical bandgap of MgO substrate (7.8

eV) [31]. All the films exhibit a high transparency of $\sim 80\%$ in the edge of the visible region and increasing Hf content does not reduce the transmittance until ~ 4.5 eV. The oscillation of spectra is due to the interference effect of film of 100 nm thickness. We extracted the optical absorption coefficient α and then estimated the optical bandgaps from Tauc plots [32],

$$(\alpha h\nu)^n = A(h\nu - E_g) \quad (2)$$

where h , ν , A , and E_g are Planck's constant, frequency, a constant, and the band gap, respectively, and n is a constant that indicates the nature of transition, which is 1/2 for indirect and 2 for direct. The extrapolated linear portion is described in Fig. 2 (b) for the direct (top) and indirect (bottom) allowed bandgaps. Most importantly, the bandgap increases with the Hf content from 3.09 eV to 5.10 eV for the indirect gap and from 3.49 eV to 5.56 eV for the direct gap.

Fig. 3 (c) compares the bandgaps of BSHO extracted from the optical transmittance spectra with the calculations based on GGA-PBEsol, where significant discrepancies exist. The smaller bandgaps of BSO and BHO in the calculated results than the measurements can be attributed to underestimation of bandgap which often occurs in PBEsol [33]. Typically, the bandgap of alloy (A_xB_{1-x}) is characterized by the bowing parameter, b [34];

$$E_g^{AB}(x) = xE_g^A + (1-x)E_g^B - bx(1-x) \quad (3)$$

Conventional semiconductors, which has p-like VBM and s-like CBM has a positive bowing parameter because very different characters between VBM and CBM makes the intraband coupling stronger than the interband coupling [35]. In the case of perovskite oxide semiconductor, the change of bandgap on the composition has not been studied in depth [36]. We speculate that the upward bowing in the calculated result of BSHO may relate to the smaller contribution of Hf-s orbital at the CBE as increasing Hf content, described in the inset of Fig. 1. The Fig. S2, illustrating the optical properties of BSHO films deposited on r-plane Al_2O_3 substrate, supports that the strain also affects the bandgap of films so that upward bowing occurs for the direct gap. Such different behavior in the bandgap with composition

in the calculations and measurements have been often observed in usual compound semiconductors [37], implying the strain effect on the band structure.

We measured the transport properties of 50 nm thick n-type BLSHO films deposited on MgO substrate with 60 nm thick BHO buffer layers. Fig. 4 (a) shows the carrier density n by Hall measurement as varying the Hf content for each La doping rate. Each horizontal dotted line indicates a 100 % activated n and it is noteworthy that in BLSOs dopants are almost fully activated, although small deviation starts at low La doping. While increasing the Hf content, the n continually decreases, as the Fermi level moves closer to the CBM. The Fermi levels apart from the CBM in Fig. 4 (b) are estimated by computing the Fermi-Dirac integral from the measured n with the effective mass of $0.42 m_0$ [38]. We found that BLSHO remains degenerate up to ~ 30 % of Hf content, suggesting the La dopants act as an effective donor despite the increased bandgap. The decreasing activation rate for Hf substitution higher than 30 % can be beneficial in controlling the tiny doping rate in heterostructures. However, the GGA-PBEsol result in Fig. S3 predicts 3.7 % La-doped $\text{BaSn}_{0.6}\text{Hf}_{0.4}\text{O}_3$ to be degenerate with $n = 2.2 \times 10^{20} \text{ cm}^{-3}$, which is in contrast to experimental results of the large resistivity of the film. More careful study for the origin of smaller La activation rate in BLSHO films, i.e, the formation energy of the cation vacancy and the La anti-site defects as well as the effect of strain, will help to realize BLSHO modulation doped layer for high mobility BSO.

In Fig. 4 (c) we plotted the electron mobility, which decreased sharply as the Hf content increases for each La doping rate although the crystallinity of the films improves with more Hf substitution, as shown in Fig. 2 (a). This reduced μ is not surprising because most of compositional alloys exhibit mobility generally lower than the linear interpolation due to alloy scattering [39], in which the fluctuations in local chemistry leads to fluctuations in electronic states. Although there is a small change of the effective mass from $0.2 m_0$ (Hf=0 %) to $0.62 m_0$ (Hf=100 %), the μ determined by both the band structure and the scattering rate sharply decreases with Hf substitution, which does not diminish its potential as

the doping layer since the transport will occur in the lower bandgap BSO layer. Our previous study on Sb doping on Sn-site also supports the large scattering on the Sn-site substitution due to the nature of SnO_6 conduction channel [38]. Fig. 4. (d) is a log-scale plot of μ as a function of the n for the Hf content of 0, 8, 21, 27 %. The strong scattering by Hf is remarkable, indicated by the vertical arrow line, showing the change of the highest μ of $95.3 \text{ cm}^2\text{V}^{-1}\text{s}^{-1}$ at $1.28 \times 10^{20} \text{ cm}^{-3}$ in BLSO to the lowest μ of $0.2 \text{ cm}^2\text{V}^{-1}\text{s}^{-1}$ at $2 \times 10^{19} \text{ cm}^{-3}$ in BLSHO with 27 % of Hf substitution. The negative slope in graph, ranging from γ values of $-0.12 \sim -0.81$ in the relation of $\mu \propto n^\gamma$, as indicated by the dotted lines, is different from the La-doped BSO and the Sb-doped BSO films in the similar n regime [1,38]. Usually, the high density of dislocations makes a bell-shaped curve [1], which results from the ineffective screening of charge traps in low doping regime coupled with strong dopant impurity scattering in high doping regime, as represented by blank red circle plots of BLSO films with BSO buffer on MgO substrate [7]. In BLSHO the ionized impurity scattering seems stronger than in BLSO, which probably shifted the dome in the bell-shaped curve toward the lower n regime. It is worth noting that, despite the large amount of Hf substitution in Sn-O-Sn conduction channel, low μ and n values can be measured in the Hall measurement, which is difficult in the case of BLSO film due to large resistivity below $n \sim 1 \times 10^{19} \text{ cm}^{-3}$. This may imply that appropriate lattice-matched grading by BSHO on MgO substrate may enhance electron transport in low doping regime of BLSO.

In summary, we deposited BSHO films epitaxially on MgO substrate and investigated the structural and optical properties as well as the transport properties of n-type BLSHO films by La doping. The high crystallinity is confirmed by X-ray diffraction and the Hf substitution systematically enlarges the lattice constant. The bandgaps from the optical transmission spectra increase with Hf without creating any mid-gap states, as predicted by the DFT calculations. The Hall measurement data indicate that BLSHO is degenerate up to ~ 30 % of Hf and μ sharply decreases. BLSHO has a potential for an appropriate modulation doping layer for the high mobility BSO.

SUPPLEMENTARY MATERIAL

See supplementary material for optical transmission spectra of 50 nm $\text{BaSn}_{1-x}\text{Hf}_x\text{O}_3$ ($x=0, 0.25, 0.5, 0.75, 1$) films with 5 nm MgO buffer layer grown on $r\text{-Al}_2\text{O}_3$ substrate, and the band structure of BLSHO ($3\times 3\times 3$) supercell by GGA-PBEsol.

ACKNOWLEDGMENTS

This work is partially supported by Samsung Science and Technology Foundation under Project No. SSTF-BA1402-09. This material is also based upon work supported by the Air Force Office of Scientific Research under award number FA9550-16-1-0192.

References

1. H. J. Kim, U. Kim, H. M. Kim, T. H. Kim, H. S. Mun, B.-G. Jeon, K. T. Hong, W.-J. Lee, C. Ju, K. H. Kim, and K. Char, High mobility in a stable transparent perovskite oxide, *Appl. Phys. Express* **5**, 061102 (2012)
2. H. J. Kim, U. Kim, T. H. Kim, J. Kim, H. M. Kim, B.-G. Jeon, W.-J. Lee, H. S. Mun, K. T. Hong, J. Yu, K. Char, and K. H. Kim, Physical properties of transparent perovskite oxides (Ba,La)SnO₃ with high electrical mobility at room temperature, *Phys. Rev. B* **86**, 165205 (2012)
3. P. V. Wadekar, J. Alaria, M. O'Sullivan, N. L. O. Flack, T. D. Manning, L. J. Phillips, K. Durose, O. Lozano, S. Lucas, J. B. Claridge, and M. J. Rosseinsky, Improved electrical mobility in highly epitaxial La:BaSnO₃ films on SmScO₃(110) substrates, *Appl. Phys. Lett.* **105**, 052104 (2014)
4. Z. Lebens-Higgins, D. O. Scanlon, H. Paik, S. Sallis, Y. Nie, M. Uchida, N. F. Quackenbush, M. J. Wahila, G. E. Sterbinsky, D. A. Arena, J. C. Woicik, D. G. Schlom, and L. F. J. Piper, Direct observation of electrostatically driven band gap renormalization in a degenerate perovskite transparent conducting oxide, *Phys. Rev. Lett.* **116**, 027602 (2016)
5. W.-J. Lee,¹H. J. Kim, E. Sohn,T. H. Kim, J.-Y. Park, W. Park, H. Jeong, T. Lee, J. H. Kim, K.-Y. Choi, and K. H. Kim, Enhanced electron mobility in epitaxial (Ba,La)SnO₃ films on BaSnO₃(001) substrates, *Appl. Phys. Lett.* **108**, 082105 (2016)
6. H. Paik, Z. Chen, E. Lochocki, A. Seidner H., A. Verma, N. Tanen, J. Park, M. Uchida, S. Shang, B.-C. Zhou, M. Brutzam, R. Uecker, Z.-K. Liu, D. Jena, K. M. Shen, D. A. Muller, and D. G. Schlom, High-mobility BaSnO₃ grown by oxide molecular beam epitaxy, *APL Mater.* **5**,116107 (2017)
7. J. Shin, Y. M. Kim, Y. Kim, C. Park, and K. Char, High mobility BaSnO₃ films and field effect transistors on non-perovskite MgO substrate, *Appl. Phys. Lett.* **109**, 262102 (2016)
8. H. Mun, U. Kim, H. M. Kim, C. Park, T. H. Kim, H. J. Kim, K. H. Kim, and K. Char, Large effects of dislocations on high mobility of epitaxial perovskite Ba_{0.96}La_{0.04}SnO₃ films, *Appl. Phys. Lett.* **102**, 252105 (2013)
9. K. Ganguly, P. Ambwani, P. Xu, J. S. Jeong, K. A. Mkhoyan, C. Leighton, and B. Jalan, Structure and transport in high pressure oxygen sputter-deposited BaSnO_{3-δ}, *APL Mater.* **3**, 062509 (2015)
10. C. Park, U. Kim, C. J. Ju, J. S. Park, Y. M. Kim, and K. Char, High mobility field effect transistor based on BaSnO₃ with Al₂O₃ gate oxide, *Appl. Phys. Lett.* **105**, 203503 (2014)
11. Y. M. Kim, C. Park, U. Kim, C. Ju, and K. Char, High-mobility BaSnO₃ thin-film transistor with HfO₂ gate insulator, *Appl. Phys. Express* **9**, 011201 (2016)

12. Y. M. Kim, C. Park, T. Ha, U. Kim, N. Kim, J. Shin, Y. Kim, J. Yu, J. H. Kim, and K. Char, High-k perovskite gate oxide BaHfO₃, *APL Mater.* **5**, 016104 (2017)
13. U. Kim, C. Park, T. Ha, Y. M. Kim, N. Kim, C. Ju, J. Park, J. Yu, J. H. Kim, and K. Char, All-perovskite transparent high mobility field effect using epitaxial BaSnO₃ and LaInO₃, *APL Mater.* **3**, 036101 (2015)
14. K. Fujiwara, K. Nishihara, J. Shiogai, and A. Tsukazaki, Enhanced electron mobility at the two-dimensional metallic surface of BaSnO₃ electric-double-layer transistor at low temperatures, *Appl. Phys. Lett.* **110**, 203503 (2017)
15. S. Rajan, H. Xing, S. Denbaars, and U. K. Mishra, AlGaIn/GaN polarization-doped field-effect transistor for microwave power applications, *Appl. Phys. Lett.* **84**, 1591 (2004)
16. T. Mimura, S. Hiyamizu, T. Fujii, and K. Nanbu, A new field-effect transistor with selectively doped GaAs/n-Al_xGa_{1-x}As heterojunctions, *Jpn. J. Appl. Phys.* **19**, L225 (1980)
17. T. Mimura, S. Hiyamizu, K. Joshin, and K. Hikosaka, Enhancement-mode high electron mobility transistors for logic applications, *Jpn. J. Appl. Phys.* **20**, L317 (1981)
18. P. M. Solomon and H. Morkoc, Modulation-doped GaAs/AlGaAs heterojunction field-effect transistors (MODFET's), ultrahigh-speed device for supercomputers, *IEEE Trans. Electron Devices* **31**, 1015 (1984)
19. G. Bersuker, P. Zeitzoff, G. Brown, and H. R. Huff, Dielectrics for future transistors, *Materials Today* **7**, 26 (2004)
20. N. Reyren, S. Thiel, A. D. Caviglia, L. Fitting Kourkoutis, G. Hammerl, C. Richter, C. W. Schneider, T. Kopp, A.-S. Ruetschi, D. Jaccard, M. Gabay, D. A. Muller, J. -M. Triscone, and J. Mannhart, Superconducting interfaces between insulating oxides, *Science* **317**, 1196 (2007)
21. H. Mizoguchi, H. W. Eng, and P. M. Woodward, Probing the electronics structures of ternary perovskite and pyrochlore oxides containing Sn⁴⁺ or Sb⁵⁺, *Inorganic Chemistry* **43**, 1667 (2004)
22. H. Wang, X. Jiao, Q. Liu, X. Xuan, F. Chen, and W. Wu, Transparent and conducting oxide films of the perovskite La_xSr_{1-x}SnO₃ (x ≤ 0.15): epitaxial growth and application for transparent heterostructures, *J. Phys. D: Appl. Phys.* **43**, 035403 (2010)
23. B. Hadjarab, A. Bouguelia, and M. Trari, Synthesis, physical and photo electrochemical characterization of La-doped SrSnO₃, *J. Phys. Chem. Solids* **68**, 1491 (2007)
24. E. Baba, D. Kan, Y. Yamada, M. Haruta, H. Kurata, Y. Kanemitsu, and Y. Shimakawa, Optical and transport properties of transparent conducting La-doped SrSnO₃ thin films, *J. Phys. D: Appl. Phys.* **48**, 455106 (2015)
25. Q. Liu, B. Li, J. Liu, H. Li, Z. Liu, K. Dai, G. Zhu, P. Zhang, F. Chen, and J. Dai, Structure and band gap tuning of transparent (Ba_{1-x}Sr_x)SnO₃ thin films epitaxially grown on

MgO substrates, EPL **98**, 47010 (2012)

26. G. Kresse and J. Furthmüller, Efficient iterative schemes for *ab initio* total-energy calculations using a plane-wave basis set, Phys. Rev. B **54**, 11169 (1996)

27. N. Charles and J. M. Rondinelli, Assessing exchange-correlation functional performance for structure and property predictions of oxyfluoride compounds from first principles, Phys. Rev. B **94**, 174108 (2016)

28. L. Abbes and H. Noura, Perovskite oxides MRuO₃ (M = Sr, Ca and Ba): Structural distortion, electronic and magnetic properties with GGA and GGA-modified Becke–Johnson approaches, Results in Physics **5**, 38 (2015)

29. H.-R. Liu, J.-H. Yang, H. J. Xiang, X. G. Gong, and S.-H. Wei, Origin of the superior conductivity of perovskite Ba(Sr)SnO₃, Appl. Phys. Lett. **102**, 112109 (2013)

30. L. Vegard, Die constitution der mischkristalle and die raumfullung der aotmem Z. Phys. **5**, 17 (1921)

31. D. M. Roessler and W. C. Walker, Electronic spectrum and ultraviolet optical properties of crystalline MgO, Phys. Rev. **159**, 733 (1967)

32. J. Tauc, R. Grigorovici, and A. Bancu, Optical properties and electronic structure of amorphous germanium, Phys. Stat. Sol. **15**, 627 (1966)

33. C. Franchini, Hybrid functionals applied to perovskites, J. Phys. : Condens. Matter **26**, 253202 (2014)

34. J. Wu, W. Walukiewicz, K. M. Yu, J. W. Ager III, S. X. Li, E. E. Haller, H. Lu, and W. J. Schaff, Universal bandgap bowing in group-III nitride alloys, Solid State Communications **127**, 411 (2003)

35. Zhiming M. Wang, MoS₂: Materials, Physics, and Devices (Springer, Switzerland, 2014)

36. T. Schumann, S. Raghavan, K. Ahadi, H. Kim, and S. Stemmer, Structure and optical band gaps of (Ba,Sr)SnO₃ films grown by molecular beam epitaxy, J. Vac. Sci. Technol. A **34**, 050601 (2016)

37. K. Kim, G. L. W. Hart, and A. Zunger, Negative band gap bowing in epitaxial InAs/GaAs alloys and predicted band offsets of the strained binaries and alloys on various substrates, Appl. Phys. Lett. **80**, 3105 (2002)

38. U. Kim, C. Park, T. Ha, R. Kim, H. S. Mun, H. M. Kim, H. J. Kim, T. H. Kim, N. Kim, J. Yu, K. H. Kim, J. H. Kim, and K. Char, Dopant-site-dependent scattering by dislocations in epitaxial films of perovskite semiconductor BaSnO₃, APL Mater. **2**, 056107 (2014)

39. Angus Rockett, The Materials Science of Semiconductors (Springer, New York, 2008)

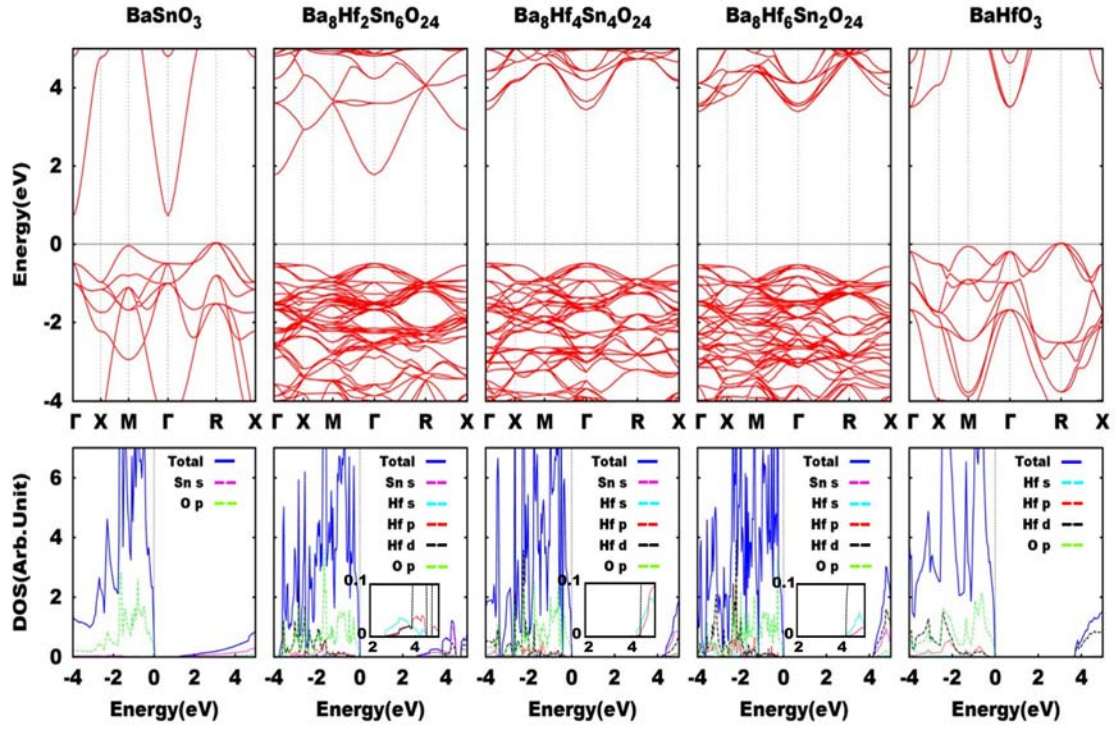


FIG. 1. Band structure (top) and total/atom resolved partial density of states (PDOS)(bottom) near the Fermi energy for $\text{BaSn}_{1-x}\text{Hf}_x\text{O}_3$ ($x=0, 0.25, 0.5, 0.75, 1$) as obtained from DFT calculations with GGA-PBESol exchange correlation functional. The $2 \times 2 \times 2$ supercell is used for $\text{BaSn}_{1-x}\text{Hf}_x\text{O}_3$ ($x=0.25, 0.5, 0.75$). The effective masses of conduction band are 0.2, 0.28, 0.36, 0.41, 0.62 m_0 , respectively. The TDOS of $\text{BaSn}_{1-x}\text{Hf}_x\text{O}_3$ ($x=0.25, 0.5, 0.75$) is scaled down to 1/8 in each graph to show each orbital character effectively. The inset is the enlarged PDOS plot for Hf orbitals.

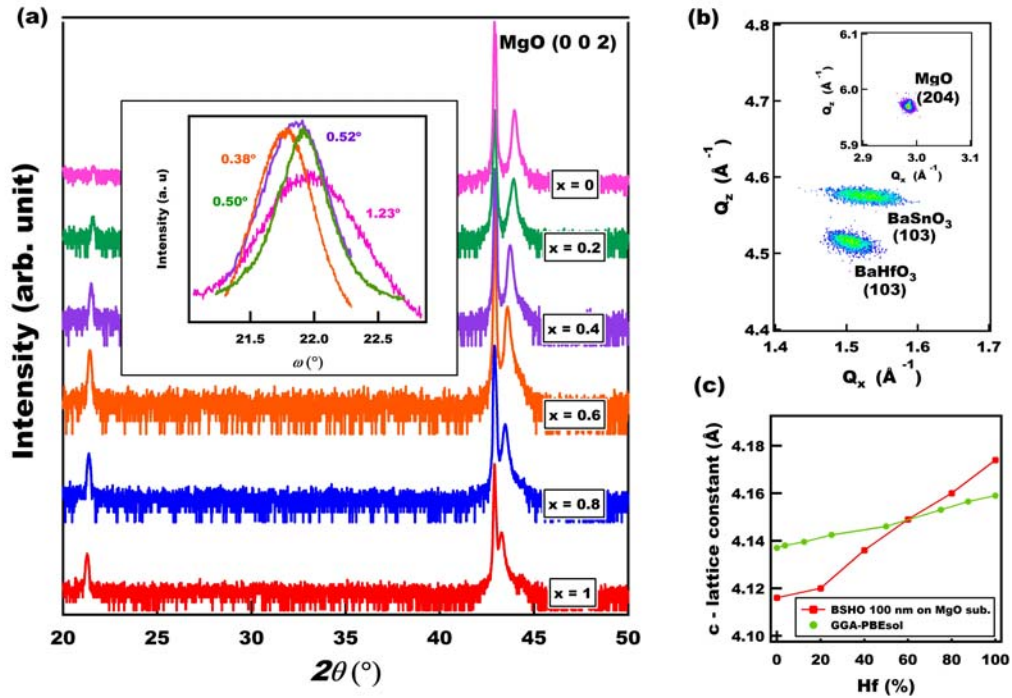


FIG. 2. X-ray diffraction patterns of BSHO films grown on [001] MgO substrate. (a) $\theta-2\theta$ scans of BaSn_{1-x}Hf_xO₃ ($x=0, 0.2, 0.4, 0.6, 0.8, 1$) and its rocking curves of BaSn_{1-x}Hf_xO₃ ($x=0, 0.2, 0.4, 0.6$) around (002) peaks. (b) Reciprocal space map around the (103) Bragg reflection of each BSO and BHO films and the (204) reflection of MgO substrate. (c) the lattice constant from $\theta-2\theta$ scans and the calculation based on GGA-PBEsol as a function of the Hf content.

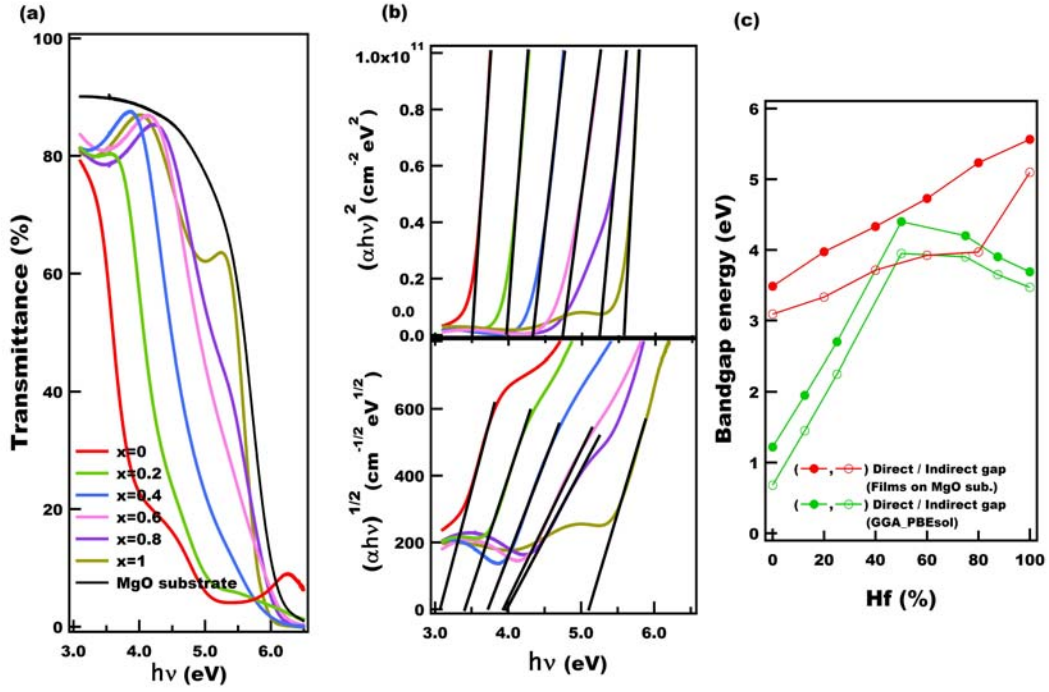


FIG. 3. Optical transmission spectra of BSHO films grown on [001] MgO substrate. (a) Optical transmittance of $\text{BaSn}_{1-x}\text{Hf}_x\text{O}_3$ ($x=0, 0.2, 0.4, 0.6, 0.8, 1$) films. (b) $(\alpha h\nu)^2$ vs. $h\nu$ plot and $(\alpha h\nu)^{1/2}$ vs. $h\nu$ plot. The bandgap energy is extrapolated from the linear line. (c) Direct and indirect bandgap energy as varying the Hf content from the optical transmission spectra and the calculations based on GGA-PBEsol.

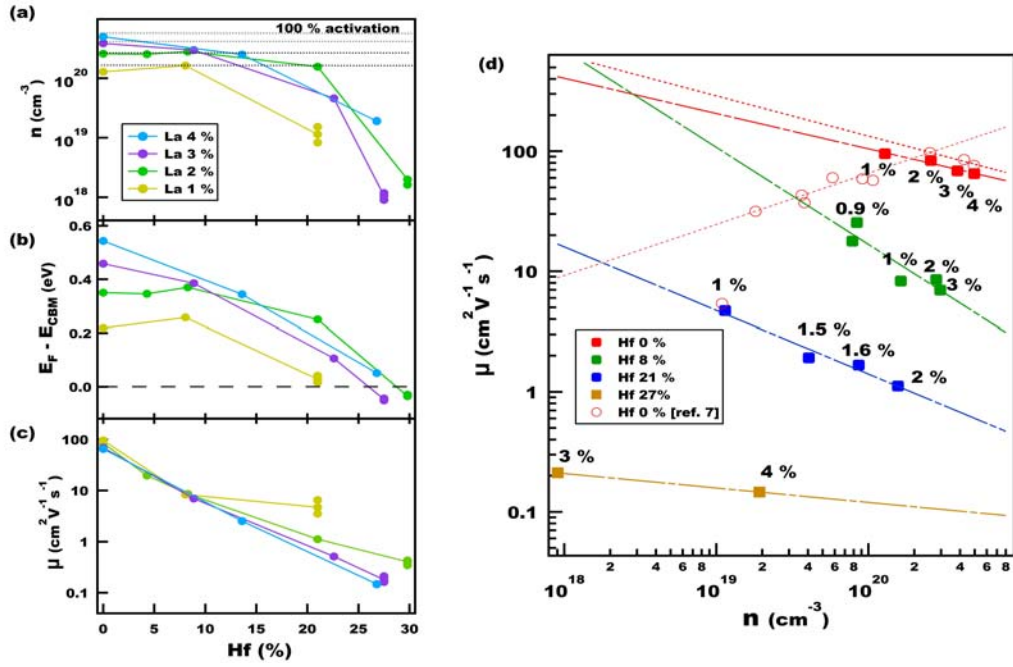


FIG. 4. Transport properties of 50 nm BLSHO films with 60 nm BHO buffer layer grown on [001] MgO substrate. (a) The carrier concentration as a function of the Hf content in each La doping rate. The dotted lines are fully activated carrier density in each La doping rate. (b) The Fermi level apart from CBM as a function of the Hf content. (c) The change of mobility as a function of the Hf content in each La doping rate. (d) The mobility as a function of the carrier concentration for each Hf content. La doping rates are denoted at each point. The γ value of the dotted line in $\mu \propto n^\gamma$, is -0.29, -0.81, -0.53, -0.12, respectively, for Hf 0 %, 8 %, 21 %, and 27 % substitution. The blank red circle is data of BLSO films (50 nm) with BSO buffer (150 nm) on MgO substrate from ref. 7.